Quantification of the Strength of π-Noncovalent Interactions in Molecular Balances using Density Functional Methods

Luka Nunar and Abil E. Aliev*[a]

Different molecular balances were designed previously to compare noncovalent interactions. However, some balances are difficult to synthesise and there is a need for developing a computational approach. In this work, we probe noncovalent interactions of π systems using DFT methods to assess their reliability in reproducing experimentally measured conformer populations. Based on our results, the PW6B95D3 functional performed best, followed by M11L and ωB97XD. Additionally, the simulation of the rotation of the hydroxyl group revealed stabilising OH···Alkyne and OH···Nitrile interactions that are difficult to identify experimentally. These methods were then applied to compare the strengths of sulfur···π interactions in molecules which have not been explored experimentally. Compared to the hydroxyl counterpart, the simulation of the thiol group rotation showed that the geometry of the conformer with the two sulfur lone pairs oriented towards the aromatic ring or the double bond is stabilised, suggesting that S(LP)···π interactions can be attractive in nature. The ability of sulfur to rearrange its electronic surrounding to form an attractive interaction with π systems, including those with either electron-donating or withdrawing groups, was also confirmed. Overall, the results show a promising future for both qualitative and quantitative assessments of the strengths of noncovalent interactions using selected DFT techniques.

Introduction

It is a generally accepted that virtually all processes, whether chemical or biological, involve noncovalent interactions.[1–4] They determine the structural and behavioural properties of materials, affect synthesis, define the secondary and tertiary structure of protein folding, etc. They are also transmitters of stereochemical information and play a critical role in the enzyme-ligand binding and are therefore very important aspect of research in drug design.[5–8] Initially, strong noncovalent interactions, such as hydrogen bonds, were studied widely, while other weaker noncovalent interactions were often neglected.[9,10] Over the past few decades various studies have confirmed that the relatively weak noncovalent interactions of π-systems (e.g., double bonds and aromatic rings) are also important.[11] Due to their importance, multiple methods for an experimental quantification of the strength of noncovalent interactions have been developed with different levels of success in quantification of the strength of the noncovalent interactions of π-systems.[12,13] As an experimental technique,

NMR spectroscopy has been applied widely for estimating populations of conformers stabilised by noncovalent interactions.

One of the factors that prevents detailed studies of noncovalent interactions in biological systems is their very complex nature, with multiple intra- and intermolecular interactions present. It is therefore impossible to detect and quantify particular noncovalent interactions individually. Another issue is the relative weakness of the interactions. When present in the system, they are often too weak to overcome the entropic penalty that comes with the formation of structures stabilised by noncovalent interactions. Lastly, it is difficult to identify the geometry of each interaction in complex systems with a large number of atoms.[1,13] In order to evaluate individual interactions quantitatively, certain small molecules have been designed experimentally for the express purpose of helping to sort out the interactions. These are known as molecular balances and usually have limited degrees of conformational freedom which allow the system to reach a molecular geometry where the noncovalent interaction of interest can be observed intra-molecularly which eliminates or at least minimises potential interference from steric, solvent and other intramolecular interactions that might be present. There are multiple different classes of molecular balances, most notably a series of triptycenes of Ōki,[14] aryl esters of Wilcox,[15–17] biaryls of Cozzi,[18–20] N-arylimides of Verma and Singh,[21] aromatic balances of Jennings[22,23] and formamides of Cockroft.[24] Each of these balances was usually designed for studying specific noncovalent interactions and their strength.[14–24] In this work, we will focus on bicyclononane balances designed by Mother-well et al.,[25–29] in which the dibenzobicyclo[3.2.2.]nonane is used as the base for a molecular framework where by changing

[a] L. Nunar, Dr. A. E. Aliev
Department of Chemistry
University College London
20 Gordon Street
London WC1H 0AJ (UK)
E-mail: A.E.Aliev@ucl.ac.uk

Chemistry—Methods

Research Article
doi.org/10.1002/cmtd.202200044

Chemistry Europe
European Chemical
Societies Publishing

two functional groups Y and Z that are attached to the central carbon of the 9,10-propano bridge Z⋯Arene and Y⋯Arene interactions can be compared and ranked by strength (Figure 1).

However, it is not always possible to synthesise the balance of interest with desired Z and Y substituents experimentally. There is therefore a need for an alternative computational approach. The objective of this work is to assess the quality and reliability of various computational methods based on density functional theory (DFT) for determining the populations of conformers stabilised by π interactions. The main advantage of this approach compared to NMR spectroscopy is that a detailed insight can be gained into molecular geometries stabilised by noncovalent interactions. Different levels of theory were compared with the available experimental results in order to choose the computational method that best reproduces the experimentally known conformer populations in the case of weak π-interactions of different functional groups with aromatic rings, as well as double and triple bonds. Furthermore, these different methods were used to simulate the full hydroxyl and thiol group rotations in molecular balances to gain a detailed insight into their one-dimensional (1D) potential energy surfaces (PES), which is not available from experimental measurements. In addition, the DDEC6 (Density Derived Electrostatic and Chemical 6)[30] method was used to evaluate the potential of this technique in detecting and evaluating the strength of noncovalent interactions. The results of the computations showed that some of the DFT methods are sufficiently accurate and robust for comparing the strength of weak π interactions in a pairwise manner. The most satisfactory levels of theory were then selected and applied to molecular balances that are hard or impossible to build experimentally, yet needed for direct pairwise comparison of functional groups.
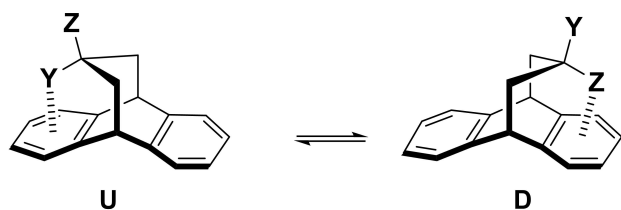
The main focus in this part of the work was on probing sulfur⋯π interactions.

Results and Discussion

The hydroxyl group rotation

We first consider the rotation of the hydroxyl group for the set of Motherwell balances shown in Figure 2 in order to estimate the number of possible conformers which could be involved in a dynamic exchange, as well as their relative energies. Previous studies have shown that the experimentally measured energetic characteristics of internal bond rotations and populations of multiple conformers involved in dynamic exchange can be well reproduced by quantum mechanical calculations.[31] The molecular balances considered here are denoted as **Y|Z**, where Y=H, Me, C≡CH (abbreviated as At), CN and **Z**=OH. Graphs included in Figures 3–6 show the energy changes (in kJ mol^{-1}) as a function of dihedral angle φ using M11L/def2-TZVP calculations on rotation about the C—O bond starting from the trans conformation with the H—O-C—H or H—O-C—C(Y) dihedral angle of φ=180° (Figure 2). The C(Y) represents the first carbon of the substituent Y attached to the molecular balance. The dihedral angle φ was decremented in steps of 5° to simulate rotation of the hydroxyl proton about the C—O bond. At each step, the dihedral angle φ was fixed with all of the remaining degrees of freedom optimised using DFT calculations. A relaxed 1D PES scan was performed in this manner and minimised energies at each step were obtained. Due to the symmetry, graphs only show half of the relaxed 1D PES (corresponding to the variation of φ between 180° and 0°). Similar calculations were also carried out at the PW6B95D3/def2-TZVP level of theory, which led to 1D PES graphs mostly similar to those at the M11L/def2-TZVP level of theory (Supporting Information, Figures S1–S8).

The H|OH balance. From the relaxed 1D PES graph shown in Figure 3, the trans conformer is the lowest energy conformer for both the OH-down and OH-up conformers.

For the OH-down conformer, the energies of the gauche rotamer relative to that of the trans rotamer are 7.8 (**1d**), 10.4 (**2d**), 8.6 (**3d**) and 11.2 (**4d**) kJ mol^{-1}. The eclipsed conformation as the transition state between two gauche rotamers at φ=0° is the highest in energy for the OH-down conformer (Figure 3a). There is also clear similarity between black (**1d**) and green (**3d**) curves, as well as blue (**2d**) and red (**4d**) curves in Figure 3a. In

Figure 1. An example of a Motherwell balance. A more electronegative Z substituent (e.g., Z=OH and Y=CH₃) determines the up (U) and down (D) notation of the two conformers shown. The 9,10-propano bridge fixes the aromatic base in place, while its central carbon flips between two positions, thus creating a balance-like structure.
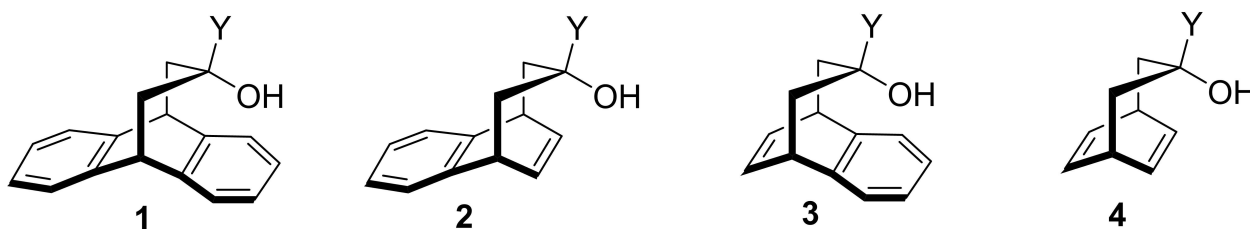

Figure 2. Motherwell balances used for simulations of the OH group rotation. The numbering of compounds is the same as in the original references.[26,27]

Chemistry—Methods

Research Article
doi.org/10.1002/cmtd.202200044

Chemistry Europe
European Chemical
Societies Publishing

Figure 3. DFT M11L/def2-TZVP simulations of the rotation about the C–O bond starting from the trans conformer of (a) **1 d-H,OH** (black), **2 d-H,OH** (blue), **3 d-H,OH** (green) and **4 d-H,OH** (red) and (b) **1 u-H,OH** (black), **2 u-H,OH** (blue), **3 u-H,OH** (green) and **4 u-H,OH** (red).
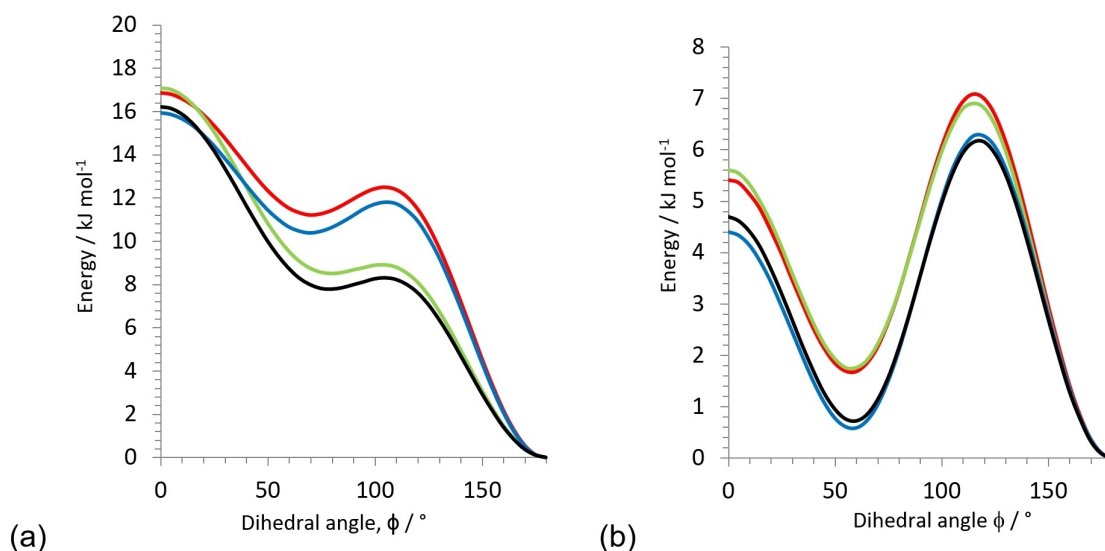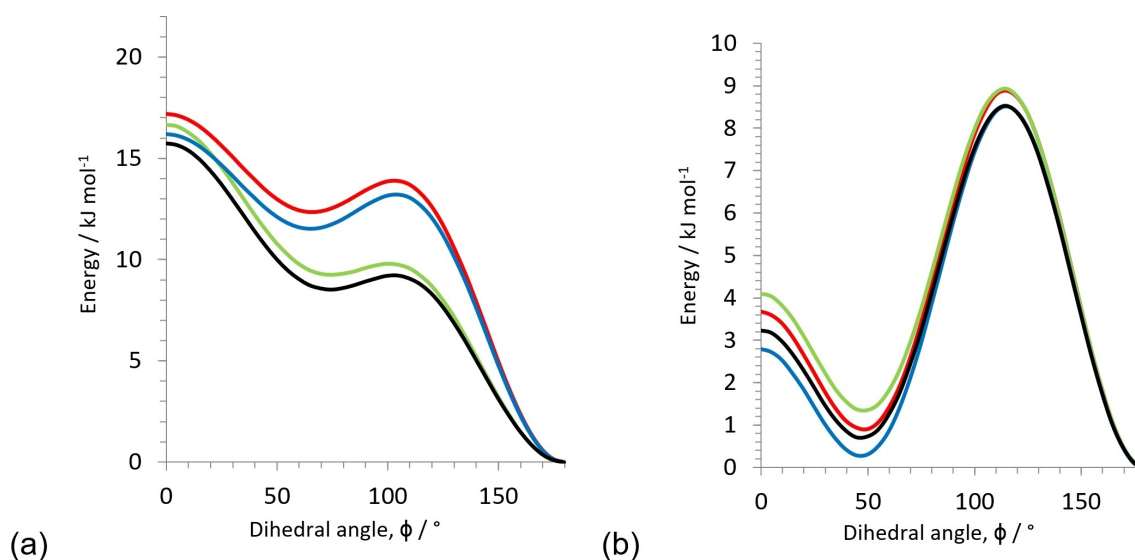

Figure 4. DFT M11L/def2-TZVP simulations of the rotation about the C–O bond starting from the trans conformer of (a) **1 d-Me,OH** (black), **2 d-Me,OH** (blue), **3 d-Me,OH** (green) and **4 d-Me,OH** (red) and (b) **1 u-Me,OH** (black), **2 u-Me,OH** (blue), **3 u-Me,OH** (green) and **4 u-Me,OH** (red).

1 d and **3 d** the OH group is placed above the benzene ring, while in **2 d** and **4 d** it is placed above the double bond. Thus, the observed grouping of the curves suggests distinctive and significant contributions from OH···Arene and OH···Alkene interactions into the 1D PES profiles. Similarly, in 1D PES graphs for OH-up conformers (Figure 3b) black (**1 u**)/blue (**2 u**) and green (**3 u**)/red (**4 u**) curves are grouped together, confirming that contributions from H···Arene and H···Alkene interactions are distinctive and significant. In **1 u** and **2 u**, the H atom in the Y position is placed in the close proximity of the benzene ring, whereas in **3 u** and **4 u** it is placed in the close proximity of the double bond.

From Figure 3a for the OH-up conformer, the energies of the gauche rotamer relative to that of the trans rotamer are 0.8

(**1 u**), 0.6 (**2 u**), 1.8 (**3 u**) and 1.8 (**4 u**) kJ mol^{-1}. These are significantly smaller than the corresponding values for the OH-down conformers (see above). The differences in relative energies are: 7.0 (**1 d–1 u**), 9.8 (**2 d–2 u**), 6.8 (**3 d–3 u**), 9.4 (**4 d–4 u**) kJ mol^{-1}. These changes clearly indicate to significant OH···Arene and OH···Alkene stabilising interactions in trans OH-down conformers and the above differences in relative energies can be considered as quantitative estimates of OH···Arene and OH···Alkene interactions by the M11L/def2-TZVP method.

The Me|OH balance. As with the H|OH balance, the trans rotamer is the lowest energy conformer for both OH-down and OH-up conformers (Figure 4).
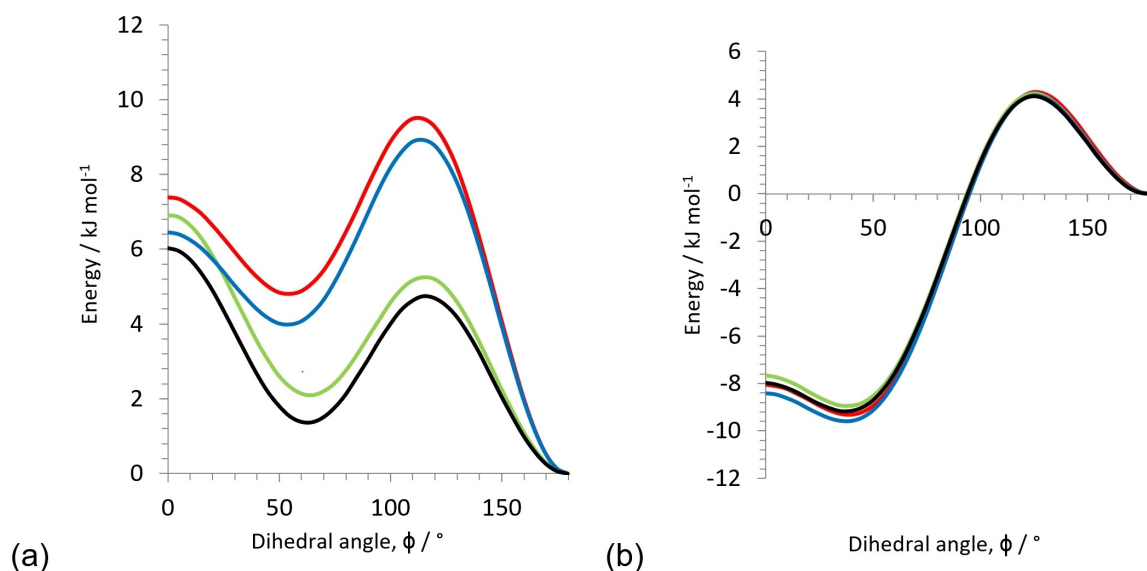
Chemistry—Methods

Research Article
doi.org/10.1002/cmtd.202200044

Chemistry Europe
European Chemical
Societies Publishing

Figure 5. DFT M11L/def2-TZVP simulations of the rotation about the C–O bond starting from the trans conformer of (a) **1 d-At,OH** (black), **2 d-At,OH** (blue), **3 d-At,OH** (green) and **4 d-At,OH** (red) and (b) **1 u-At,OH** (black), **2 u-At,OH** (blue), **3 u-At,OH** (green) and **4 u-At,OH** (red).
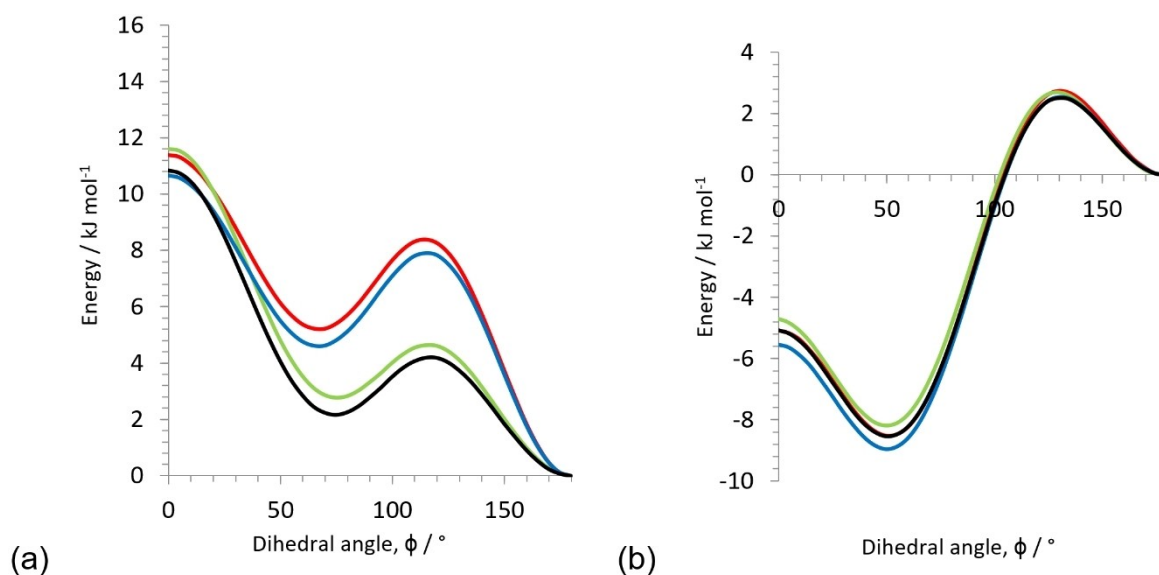

Figure 6. DFT M11L/def2-TZVP simulations of the rotation about the C–O bond starting from the trans conformer of (a) **1 d-CN,OH** (black), **2 d-CN,OH** (blue), **3 d-CN,OH** (green) and **4 d-CN,OH** (red) and (b) **1 u-CN,OH** (black), **2 u-CN,OH** (blue), **3 u-CN,OH** (green) and **4 u-CN,OH** (red).

For the OH-down conformer, the energies of the gauche rotamer relative to that of the trans rotamer are 8.5 (**1 d**), 11.5 (**2 d**), 9.3 (**3 d**) and 12.4 (**4 d**) kJ mol^{-1}. These are slightly higher than the corresponding values for the H|OH balances. It is also clear from Figure 4a, that black (**1 d**) and green (**3 d**) curves, as well as blue (**2 d**) and red (**4 d**) curves follow the same trend in pairs as in H|OH balances. From Figure 4a, the energies of the OH-up conformers of the gauche rotamer relative to that of the trans rotamer are 0.7 (**1 u**), 0.3 (**2 u**), 1.4 (**3 u**) and 0.9 (**4 u**) kJ mol^{-1}. The differences in relative energies are: 7.8 (**1 d–1 u**), 11.2 (**2 d–2 u**), 7.9 (**3 d–3 u**), 11.5 (**4 d–4 u**) kJ mol^{-1}. As in the H| OH model, these values point towards significant OH···Arene

and OH···Alkene stabilising interactions in trans OH-down conformers in Me|OH balances.

The At|OH balance. The trans rotamer was again the lowest in energy in the OH-down conformer (Figure 5). The energies of the gauche rotamer relative to that of the trans rotamer in the OH-down conformer are 1.4 (**1 d**), 4.0 (**2 d**), 2.1 (**3 d**) and 4.8 (**4 d**) kJ mol^{-1}. The significant decrease in these values compared to the Me|OH balances are indicative of an OH···Alkyne stabilising interaction between the hydroxyl proton and the C≡CH group in At|OH balances. This interaction of the hydroxyl hydrogen atom could be with the triple bond or the quaternary α carbon atom (C$^{\alpha}$) of the acetylene fragment. For H|OH models (Figure 3), the energies of the gauche rotamer relative to the

Chemistry—Methods

Research Article
doi.org/10.1002/cmtd.202200044

Chemistry Europe
European Chemical
Societies Publishing

trans rotamer were 7.8 (**1 d**), 10.4 (**2 d**), 8.6 (**3 d**) and 11.2 (**4 d**) kJ mol^{-1} at M11L/def2-TZVP level. These values suggest that the gauche rotamer is more stable in At│OH compared to H│OH by 6.4 (**1 d**), 6.4 (**2 d**), 6.5 (**3 d**) and 6.4 (**4 d**) kJ mol^{-1}. Thus, the stabilising energy of the OH···Alkyne interaction relative to that of the OH···H interaction can be estimated to be ~6.4 kJ mol^{-1} at the M11L/def2-TZVP level of theory.

The important difference is observed in 1D PES graphs for OH-up conformers (Figure 5b). The trans rotamer is not the lowest in energy anymore and is replaced by the gauche rotamer. Also, the eclipsed rotamer (between two gauche rotamers at $\varphi = 0°$) is lower in energy than the trans rotamer by ~8 kJ mol^{-1} (the average value for all 4 molecular balances considered). This is due to the OH···Alkyne interaction being present where the hydrogen atom of the OH group interacts favourably with the C≡CH fragment (i.e., attractive OH···π(At) or OH···C$^\alpha$(At) interactions or both). Another observed feature is that the curves almost perfectly overlap in the models **1 u** and **4 u** near the gauche minima, while two other minima for **2 u** and **3 u** are only slightly different from those for **1 u** and **4 u**. The examination of the structures of gauche rotamers suggest that there is likely a significant stabilising OH···Alkyne interaction at $\varphi \approx 40°$. This interaction must be relatively strong compared to the Alkyne···Arene or Alkyne···Alkene interactions, as no black/blue and red/green graph pairings are observed for OH│At (Figure 5) unlike H│OH (Figure 3). Alternatively, C≡CH···Alkene and C≡CH···Arene interactions are similar in energy in OH│At models considered, unlike H···Alkene and H···Arene interactions for H│OH substitution.

From Figure 5a, the energies of the gauche rotamer relative to that of the trans rotamer are −9.2 (**1 u**), −9.6 (**2 u**), −8.9 (**3 u**) and −9.3 (**4 u**) kJ mol^{-1}. These values are much lower than the corresponding values for the OH-down conformers due to the OH···Alkyne interaction that was not present in the H│OH and Me│OH models before. The experimental results suggest that there is a significant decrease in the population of the OH-down conformer in At│OH compared to Me│OH. The results presented in Figure 5 allow us to attribute this decrease to the presence of OH···Alkyne interactions in OH-up conformers competing well with the OH···Arene and OH···Alkene interactions in OH···down conformers.

The CN│OH balance. From Figure 6a, the trans conformer with the hydroxyl hydrogen atom placed above either the aromatic ring or the double bond of the molecular balance is the lowest in energy in OH-down conformers. The energies of the gauche rotamer relative to that of the trans rotamer are 2.2 (**1 d**), 4.6 (**2 d**), 2.8 (**3 d**) and 5.2 (**4 d**) kJ mol^{-1}. Compared to the H│OH models, the energies of the gauche rotamer relative to that of the trans rotamer are decreased by 5.6 (**1 d**), 5.8 (**2 d**), 5.8 (**3 d**) and 6.0 (**4 d**) kJ mol^{-1}. Thus, we estimate the stabilising energy of the OH···Nitrile interaction relative to that of the OH···H interaction to be ~5.8 kJ mol^{-1} at the M11L/def2-TZVP level of theory. This is only slightly less than that for the OH···Alkyne interaction (6.4 kJ mol^{-1}).

The average free energy of activation for the trans-to-gauche transition in **2 d** and **4 d** (~8.2 kJ mol^{-1}), where the OH is located above the double bond, is significantly higher than that

in **1 d** and **3 d** (~4.4 kJ mol^{-1}), where the OH group is located above the benzene ring. Similar trends were also above for the At│OH models (Figure 5).

Similar to At│OH balances, the energies of gauche rotamers at $\varphi \approx 50°$ are significantly lower compared to trans rotamers in 1D PES graphs for OH-up conformers (Figure 6b) which is attributed to the contribution from the attractive OH···Nitrile interaction. The energies of the gauche rotamer relative to that of the trans rotamer are −8.5 (**1 u**), −9.0 (**2 u**), −8.2 (**3 u**) and −8.5 (**4 u**) kJ mol^{-1}. These values indicate to relatively strong OH···Nitrile interactions, which are slightly weaker than OH···Alkyne interactions.

Analysis of conformer populations

The geometries of gauche and trans rotamers corresponding to minima on 1D PES graphs were extracted and fully optimised with no restrictions imposed. The sum of electronic and thermal free energies were calculated for the model molecules in different conformations and were used to calculate the % populations of the OH-down and OH-up conformers using a 6-site exchange model involving trans and gauche conformers (illustrated for **1-Me,OH** in Figure 7).

The calculated populations of OH-down conformers at different levels of theory were compared with the experimental results.[27,28] The root mean square (RMS, in %) deviations were calculated for each of the functional group combinations. The results are included in Table 1. On comparing two different sets of M06-2X, M11L and PW6B95D3 calculations, only relatively small changes in the RMS deviation was observed upon changing the basis set. For the Me│OH balances the results show that PW6B95D3/def2-TZVP calculations reproduce particularly well the experimental results with RMS as small as 1.4 %. However, it is important to note that the difference in RMS deviations for different levels of theory is significantly less for Me│OH balances compared to H│OH balances. In the case of At│OH balance, PW6B95D3/def2-TZVP performs the best again, though with the RMS value of 12.3 % being relatively high. The results for CN│OH balances show that M11L/def2-TZVP calculations outperform other levels of theory with an RMS value of
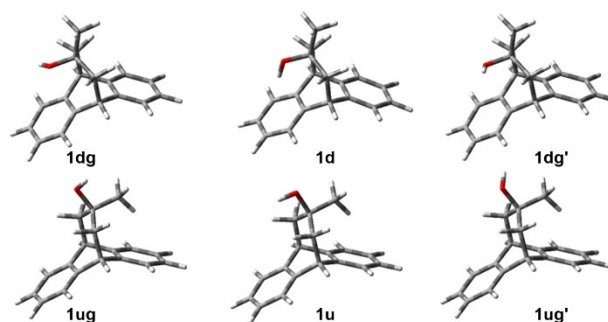

Figure 7. Trans (**1 d** and **1 u**) and gauche (**1 dg**, **1 dg**′, **1 ug**, **1 ug**′) conformers of **1-Me,OH**. In the trans conformer, the dihedral angle (φ) **H−O−C−CH₃** is 180°.

Chemistry—Methods

Research Article
doi.org/10.1002/cmtd.202200044

Chemistry Europe
European Chemical
Societies Publishing

Table 1. Percentage populations of OH-down conformers for molecular balances[26] estimated at different levels of theory at 298.15 K. The experimental values shown were measured at the same temperature.

	M11L def2-TZVP	M11L def2-QZVPP	M06-2X 6-31+G(d)	M06-2X def2-TZVP	ωB97XD def2-TZVP	PW6B95D3 def2-TZVP	PW6B95D3 def2-QZVPP	MN15 def2-TZVP	Exper. p_D, %
H|OH 1d	2.9	2.9	15.1	10.7	11.9	9.1	7.4	12.1	6.4
H|OH 2d	1.8	1.7	3.8	4.1	3.4	4.4	3.5	4.0	4.6
H|OH 3d	8.3	8.6	35.5	30.2	28.2	25.3	21.7	34.2	12.7
H|OH 4d	4.6	3.7	18.2	19.2	10.9	12.0	9.8	12.3	8.7
RMS$_H$, %	3.7	4.0	13.1	10.4	8.3	7.6	4.6	11.3	
Me|OH 1d	90.3	89.8	96.0	95.6	92.9	95.1	93.9	94.9	93.5
Me|OH 2d	83.3	80.7	87.1	87.5	85.6	90.1	87.9	87.9	92.4
Me|OH 3d	99.4	99.4	99.7	99.6	99.5	99.5	99.4	99.4	98.8
Me|OH 4d	98.3	98.1	99.1	99.0	98.6	99.0	98.9	98.9	98.9
RMS$_{Me}$, %	4.9	6.1	3.0	2.7	3.4	1.4	2.3	2.4	
At|OH 1d	34.6	29.1	43.5	45.3	35.9	43.3	38.8	27.6	50.2
At|OH 2d	14.5	12.3	15.1	20.1	23.2	24.9	21.5	9.3	44.3
At|OH 3d	57.5	52.0	84.5	82.8	77.9	75.7	74.1	79.6	71.1
At|OH 4d	38.2	33.9	55.2	55.7	64.7	56.3	53.9	51.1	68.8
RMS$_{At}$, %	23.7	27.6	17.8	15.1	13.3	12.3	14.8	23.0	
CN|OH 1d	24.9	25.8	38.0	42.9	42.6	41.4	37.9	26.7	24.8
CN|OH 2d	11.6	5.2	7.9	10.6	22.1	17.7	15.2	9.1	17.8
CN|OH 3d	31.1	32.3	62.2	60.7	65.0	49.4	49.7	59.8	29.1
CN|OH 4d	15.8	15.9	23.1	26.4	34.7	27.3	27.4	24.3	[a]
RMS$_{CN}$, %	3.8	7.5	21.4	21.4	23.3	15.1	14.2	18.4	
MUE$_{avr}$[b] %	8.4	10.4	11.3	10.1	9.1	6.9	7.1	10.9	
RMS$_{avr}$[b] %	12.8	15.1	15.0	13.6	13.3	9.9	10.3	15.6	

[a] Not reported;[26] [b] The averaged value of MUE and RMS (both in %) calculated for 15 different molecular balances for which the experimental results are available. Four methods, which best predict experimental values, are highlighted in burgundy. The MUE and RMS values shown in the table above are mean errors in the percentage population of the OH-down conformer (not the mean percentage errors).

3.8% while the other levels of theory show RMS values between 7–23%.

The averaged value of RMS calculated for 15 different molecular balances, for which the experimental results are available, show that the lowest value of 9.9% is observed for PW6B95D3/def2-TZVP, followed by PW6B95D3/def2-QZVPP (10.3%), M11L/def2-TZVP (12.8%) and ωB97XD/def2-TZVP (13.3%). We have also considered mean unsigned errors (MUE, in %) in Table 1, which has been previously used by Yu et al. for comparing the performance of different DFT functionals.[32] Here again the best performing methods were:
1. PW6B95D3/def2-TZVP (MUE 6.9%);
2. PW6B95D3/def2-QZVPP (MUE 7.1%);
3. M11L/def2-TZVP (MUE 8.4%);
4. ωB97XD/ def2-TZVP (MUE 9.1%).

Since the population percentages do not scale linearly with the energy differences, we have also considered the free energy differences. In particular, the Gibbs free energy of the OH-down conformer relative to that of the OH-up conformer was considered in Table 2. Again, the best performing DFT functional in reproducing the experimental values was PW6B95D3:
1. PW6B95D3/def2-QZVPP (MUE 1.09 kJ mol^{-1});
2. PW6B95D3/def2-TZVP (MUE 1.14 kJ mol^{-1});
3. ωB97XD/ def2-TZVP (MUE 1.46 kJ mol^{-1});
4. M11L/def2-TZVP (MUE 1.67 kJ mol^{-1}).

The differences of 0.2% and 0.05 kJ mol^{-1} in MUE values above for PW6B95D3/def2-QZVPP and PW6B95D3/def2-TZVP are insignificant and do not justify a significantly more expensive PW6B95D3/def2-QZVPP calculations compared to PW6B95D3/def2-TZVP (the number of the basis functions more than doubles on changing from def2-TZVP basis set to def2-

QZVPP for the molecules considered in this work, for example, from 710 to 1590 for **1d-OH,CN**). We have nevertheless included further PW6B95D3/def2-QZVPP results for balances considered below for additional verification.

We note that the best performance of the PW6B95D3 functional was also demonstrated for the noncovalent interactions of the S66 and S66x8 databases.[32] The S66 database includes accurate interaction energies for 66 non-covalently bonded complexes at the equilibrium van der Waals geometry of the complex, whereas the S66x8 database includes the S66 database together with the interaction energies of the 66 complexes at 7 other geometries. Previously, M11L/def2-TZVP was also identified as the best method in reproducing populations of conformers stabilised by sulfur···π and oxygen···π interactions based on the comparison of 14 different methods (see Tables S5 and S6 in Ref. [29]).

In order to additionally verify the reliability of the selected methods, we have considered the relatively difficult case of the two-site conformational equilibrium between **5S/5O** and **6S/6O** (Figure 8a,b). From experimental results, the **5S** and **6S** conformers are preferred in CDCl$_3$ with the populations of 76.7% and 92.3%.[29] The calculated populations of conformers **5S** and **6S** were 65.8% and 90.4%, respectively, at the PW6B95D3/def2-TZVP level of theory (67.5% and 90.4% from PW6B95D3/def2-QZVPP calculations). The corresponding values were 67.1% and 89.2% from M11L/def2-TZVP calculations and 38.9% and 70.8% from ωB97XD/def2-TZVP calculations. Thus, except for ωB97XD/def2-TZVP results for **5S**, the selected DFT methods satisfactorily predict the preference of the sulfur atom to point towards the aromatic ring and to the double bond compared to the smaller oxygen atom. The stabilizing effect of sulfur-arene and sulfur-

Chemistry—Methods

Research Article
doi.org/10.1002/cmtd.202200044

Chemistry Europe
European Chemical
Societies Publishing

Table 2. The Gibbs free energy of the OH-down conformer ($\Delta G°$, in kJ mol^{-1}) relative to that of the OH-up conformer estimated at different levels of theory at 298.15 K. The experimental values shown were measured at the same temperature.

	M11L def2-TZVP	M11L def2-QZVPP	M06-2X 6-31+G(d)	M06-2X def2-TZVP	ωB97XD def2-TZVP	PW6B95D3 def2-TZVP	PW6B95D3 def2-QZVPP	MN15 def2-TZVP	Exper. $\Delta G°$, kJ mol^{-1}
H|OH 1d	8.71	8.74	4.27	5.25	4.96	5.70	6.27	4.91	6.64
H|OH 2d	9.87	10.08	7.99	7.83	8.28	7.63	8.23	7.88	7.51
H|OH 3d	5.94	5.85	1.48	2.08	2.31	2.68	3.18	1.62	4.77
H|OH 4d	7.50	8.06	3.72	3.56	5.20	4.93	5.50	4.88	5.82
RMSH, kJ mol^{-1}	1.88	2.07	2.30	1.90	1.57	1.23	0.91	1.87	
Me|OH 1d	−5.53	−5.38	−7.87	−7.60	−6.35	−7.32	−6.79	−7.24	−6.60
Me|OH 2d	−3.97	−3.55	−4.73	−4.82	−4.41	−5.47	−4.92	−4.92	−6.19
Me|OH 3d	−12.74	−12.53	−14.29	−13.66	−12.96	−13.31	−12.82	−12.82	−10.92
Me|OH 4d	−10.08	−9.81	−11.67	−11.30	−10.48	−11.48	−11.07	−11.07	−11.14
RMS$_{Me}$, kJ mol^{-1}	1.62	1.79	1.96	1.61	1.40	1.31	1.15	1.19	
At|OH 1d	1.58	2.20	0.65	0.47	1.43	0.67	1.12	2.39	-0.02
At|OH 2d	4.39	4.87	4.28	3.41	2.96	2.73	3.21	5.63	0.57
At|OH 3d	−0.75	−0.20	−4.20	−3.88	−3.12	−2.82	−2.60	−3.37	−2.23
At|OH 4d	1.19	1.65	−0.51	−0.57	−1.50	−0.63	−0.39	−0.11	−1.96
RMS$_{At}$, kJ mol^{-1}	2.70	3.19	2.25	1.80	1.49	1.35	1.65	3.01	
CN|OH 1d	2.73	2.62	1.21	0.71	0.74	0.87	1.22	2.50	2.75
CN|OH 2d	5.04	7.21	6.08	5.27	3.12	3.81	4.25	5.69	3.79
CN|OH 3d	1.96	1.83	−1.23	−1.08	−1.53	0.06	0.03	−0.98	2.21
CN|OH 4d	4.15	4.12	2.98	2.54	1.56	2.43	2.41	2.82	[a]
RMS$_{CN}$, kJ mol^{-1}	0.74	1.99	2.54	2.39	2.48	1.65	1.56	2.15	
MUE$_{av}$[b] kJ mol^{-1}	1.67[c]	2.06	2.00	1.67[c]	1.46	1.14	1.09	1.72	
RMS$_{av}$[b] kJ mol^{-1}	1.92	2.34	2.25	1.91	1.73	1.38	1.34	2.15	

[a] Not reported;[26] [b] The averaged value of MUE and RMS (both in kJ mol^{-1}) calculated for 15 different molecular balances for which the experimental results are available. Four methods, which best predict experimental values, are highlighted in burgundy. [c] MUE$_{av}$ values were 1.667 and 1.674 kJ mol^{-1} for M11L/def2-TZVP and M06-2X/def2-TZVP, respectively.
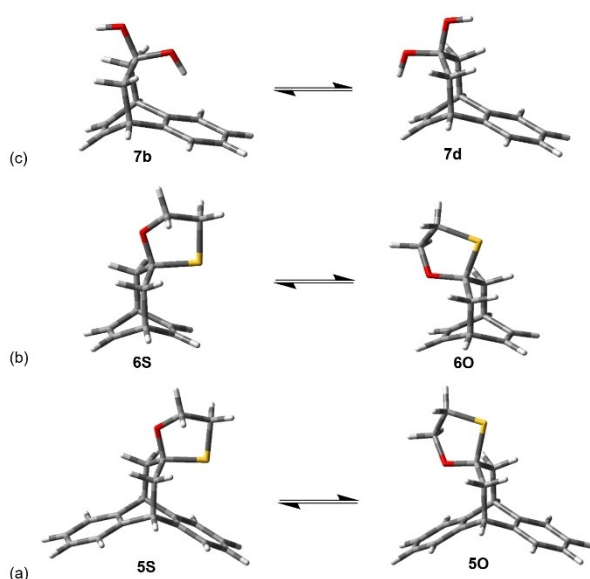

Figure 8. Conformational equilibria between (a) **5S** and **5O**; (b) **6S** and **6O** and (c) **7 b** and **7 d**.

alkene interactions can be attributed to such factors as the availability of empty 3*d*-orbitals on sulfur or to the enhanced polarizability of sulfur compared to oxygen.[29]

The selected three functionals were further tested using the hypothetical dihydroxyl derivative **7** (Figure 8c), where the subtle difference between the OH···Arene and OH···Alkene interactions is probed. From M11L/def2-TZVP calculations, the OH···Alkene interaction was preferred by 1.49 kJ mol^{-1} compared to the OH···Arene interaction (with the population of the

7 b conformer 35.4%). From PW6B95D3/def2-TZVP calculations, the OH···Arene interaction was preferred by 1.88 kJ mol^{-1} compared to the OH···Alkene interaction (with the population of the **7 b** conformer 68.1%). Similarly, from PW6B95D3/def2-QZVPP calculations, the OH···Arene interaction was preferred by 1.63 kJ mol^{-1} compared to the OH···Alkene interaction (with the population of the **7 b** conformer 65.9%). Finally, ωB97XD/def2-TZVP predicts that the OH···Arene interaction was preferred by 1.98 kJ mol^{-1} compared to the OH···Alkene interaction (with the population of the **7 b** conformer 67.0%). Previously, comparative studies of molecular balances by NMR spectroscopy showed that noncovalent interactions of the OH group with an arene dominate over those with an alkene, and that a π-facial intramolecular hydrogen bond from a hydroxy group to an arene is favoured by approximately 1.2 kJ mol^{-1}. Thus, the best performing PW6B95D3 functional (Tables 1 and 2) is in agreement with the experimental findings in this case.

Decision on the level of theory

Overall, the analysis of population calculations indicate that PW6B95D3/def2-TZVP calculations perform reasonably well in reproducing experimental results compared to other methods (Tables 1 and 2). Therefore, we have used the PW6B95D3/def2-TZVP level of theory in further calculations. Additionally, however, we have also performed M11L/def2-TZVP and ωB97XD/def2-TZVP calculations in order to further verify the conclusions reached. The computationally more expensive PW6B95D3/def2-QZVPP method was used for adjudication

Chemistry—Methods

Research Article
doi.org/10.1002/cmtd.202200044

Chemistry
Europe
European Chemical
Societies Publishing

purposes, when contradicting results were obtained by three DFT methods considered.

DDEC6 analysis

Manz used bond orders calculated by the DDEC6 method to analyse a wide range of materials, including three compounds containing hydrogen bonded water molecules: natrolite, ice crystal and ice solid surface.[30] The hydrogen bond orders in these solids were found to be in the range 0.07–0.13, while the net atomic charges of the hydrogen atoms involved in hydrogen bonds were 0.40–0.44.[30a,33] Based on these values, Manz concluded that the hydrogen bonds of water molecules in these three materials contain a significant electrostatic character and a small covalent character. Herein, we use bond order values derived from DDEC6 calculations to evaluate the strength of various noncovalent interactions which might exist in a given molecular geometry due to the proximity of certain atom pairs and how these noncovalent interactions contribute to the stability of various conformers. Atomic charges were calculated using the DDEC6 method. All structures were optimised at the PW6B95D3/def2-TZVP level of theory before charge calculations were performed. Selected bond orders derived from the DDEC6 analysis of the PW6B95D3/def2-TZVP wave functions are presented in the Table 3 (net atomic charges are included in Table S1 in Supporting Information). The non-hydrogen atoms of the Y substituents are denoted as C^α and X^β

(e.g., X=N for the CN group). The structures and atom numbering are illustrated using the OH|CN balances in Figure 9.

The values of DDEC6 bond orders for OH···C5 atom pairs are ~0.028 in **1d-Y,OH** (Y=**CN**, **At** and **Me**) and <0.0004 in **1dg-Y,OH**. In the gauche rotamers, the hydroxyl proton is placed above the C6 carbon atom of the aromatic ring and higher DDEC overlap populations are expected for the OH···C6 pair compared to the OH···C5 pair. The corresponding bond order values for OH···C6 atom pairs are ~0.028 in **1d-Y,OH** and <0.002 in **1dg-Y,OH**. Based on this analysis, noncovalent interactions of OH···C5/C6 atom are favoured significantly in **1d-Y,OH** compared to **1dg-Y,OH**. Judging by the bond order values in Table 3 for different conformers, the OH···Arene interactions form the strongest noncovalent bond in **1-At,OH**, then in **1-CN,OH** followed by **1-Me,OH**.

In conformers with the OH-up orientation, the OH···C5/C6 interactions are insignificant due to the increased distances between OH···C5/C6 atoms compared to the OH-down orientation. The interaction of the C^α atom of the CN (or At group) with the aromatic C9/C10 atoms are becoming important due to their proximity. The bond orders for C^α···C9/C10 pairs are ~0.021 in **1u-CN,OH** and **1ug-CN,OH**, ~0.021 in **1u-At,OH** and **1ug-At,OH** and ~0.011 for C^α···C9/C10 pairs in **1u-Me,OH** and **1ug-Me,OH**. A smaller bond order of ~0.003 is also detected for CN···C9/C10 pairs in **1u-CN,OH** and **1ug-CN,OH** (~0.004 for C^β···C9/C10 in **1u-At,OH** and **1ug-At,OH**). Thus, in the **1ug-CN,OH** (**1ug-At,OH**) conformer, both the OH···CN and NC···Ar-

Table 3. DDEC6 bond orders of selected atom pairs.

Conformer	C5···H	C6···H	C^α···H	X^β···H	C10···C^α	C9···C^α	C10···X^β	C9···X^β
1d-CN,OH	0.0276	0.0276	0.0001	n.d.[a]	0	0	n.d.[a]	n.d.[a]
1dg-CN,OH	0.0003	0.0017	0.0037	0.0001	0	0	n.d.[a]	n.d.[a]
1u-CN,OH	0	0	0.0001	n.d.[a]	0.0200	0.0201	0.0030	0.0030
1ug-CN,OH	n.d.[a]	n.d.[a]	0.0080	0.0004	0.0220	0.0223	0.0028	0.0027
1d-At,OH	0.0287	0.0287	0.0002	n.d.[a]	0	0	n.d.[a]	n.d.[a]
1dg-At,OH	0.0002	0.0009	0.0075	0.0003	0.0001	0.0001	n.d.[a]	n.d.[a]
1u-At,OH	0	0	0.0002	n.d.[a]	0.0198	0.0198	0.0042	0.0042
1ug-At,OH	n.d.[a]	n.d.[a]	0.0132	0.0008	0.0217	0.0215	0.0037	0.0038
1d-Me,OH	0.0271	0.0271	0.0002	n.a.[b]	0.0001	0.0001	n.a.[b]	n.a.[b]
1dg-Me,OH	0.0002	0.0011	0.0070	n.a.[b]	0.0001	0.0001	n.a.[b]	n.a.[b]
1u-Me,OH	0	0	0.0002	n.a.[b]	0.0107	0.0108	n.a.[b]	n.a.[b]
1ug-Me,OH	n.d.[a]	n.d.[a]	0.0124	n.a.[b]	0.0119	0.0116	n.a.[b]	n.a.[b]

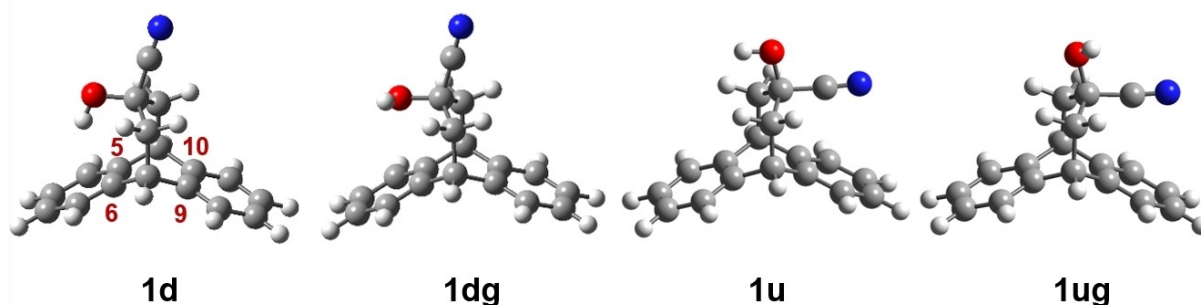[a] n.d. = not detected; [b] n.a. = not applicable because X^β = H

Figure 9. CN|OH molecular balances with carbon atoms numbered.

ene (OH···At and C$^\alpha$···Arene) interactions contribute to the molecular stability, making it the most preferred conformer. Overall, judging by the bond order values in Table 3, the OH···Arene interactions form the strongest noncovalent bond (with the bond order of ~0.028) followed by NC$^\alpha$···Arene (~0.022), HCC$^\alpha$···Arene (~0.021) and H$_3$C$^\alpha$···Arene (~0.011) interactions.

Application to previously unexplored systems

To examine the potential of the above identified DFT techniques on molecular balances which either have not been synthesised or are very difficult to synthesise, various structures were considered for assessing the strength and directionality of S···π interactions.[34] Sulfur···Arene close contacts are common in protein crystals, with the majority of the interactions being to the face of the aromatic ring.[35,36] It has been previously estimated that the S···π stabilising contributions falls between 2 and 8 kJ mol^{-1}.[37] The first example of evaluating an S···π(Arene) interaction by modulating the electrostatic surface of the arene was described by Daeffler et al.[38] It was proposed that the fluorination of the aromatic ring is expected to reduce the electron density of the aromatic ring and, therefore, will diminish the strength of the S···π(Arene) interaction, although

it was not possible to establish whether the face of the aromatic ring preferentially interacts with the sulfur lone pairs or through and SH···π interaction using experimental techniques. Here we apply the above-discussed M11L, ωB97XD and PW6B95D3 functionals to various molecular balances with S···π interactions in order to reveal the level of detail not available from experimental techniques.

A thiol group rotation in the Me|SH balance. We first consider the rotation about the C—S bond in the Me|SH derivatives of **1**–**4**. Figure 10 shows relaxed 1D PES graphs calculated at M11L/def2-TZVP, ωB97XD/def2-TZVP and PW6B95D3/def2-TZVP levels of theory. The results suggest that the stability of the eclipsed conformer has considerably improved compared to the corresponding Me|OH balances. The fully eclipsed conformer with the dihedral angle of φ(H–S–C–CH3) = 0° and the two lone pairs of the sulfur atom oriented towards the double bond in **2 d** and **4 d** balances is the lowest energy conformer, as predicted by M11L and PW6B95D3 functionals. The ωB97XD functional predicts slightly higher energy for the eclipsed rotamer relative to the trans rotamer (0.03 and 0.43 kJ mol^{-1} for **2 d** and **4 d**, respectively).

In **1 d** and **3 d** balances, the lowest energy conformers are the eclipsed rotamers according to M11L, while trans rotamers are the lowest in energy in ωb97XD and PW6B95D3 calculations. Compared to **1 d-Me,OH**, the energy of the eclipsed **1 d-**
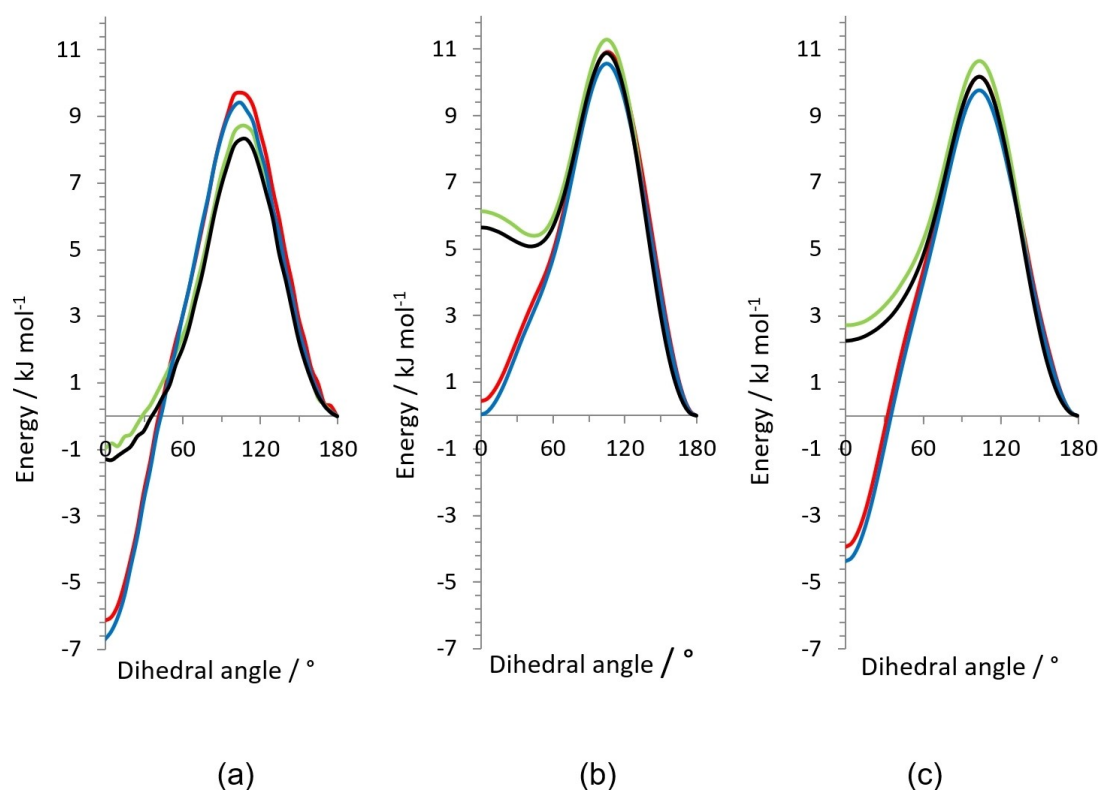

(a)   (b)   (c)

Figure 10. DFT simulations of the rotation about the C—S bond starting from the trans conformer of **1 d-Me,SH** (black), **2 d-Me,SH** (blue), **3 d-Me,SH** (green) and **4 d-Me,SH** (red) using (a) M11L/def2-TZVP, (b) ωB97XD/def2-TZVP and (c) PW6B95D3/def2-TZVP levels of theory. Similar PW6B95D3/def2-QZVPP simulations for **1 d-Me,SH** and **4 d-Me,SH** are presented in Figure S9 in Supporting Information.

Chemistry—Methods

Research Article
doi.org/10.1002/cmtd.202200044

Chemistry Europe
European Chemical
Societies Publishing

Me,SH rotamer relative to the trans **1d-Me,SH** rotamer has decreased by ~17 and ~13 kJ mol⁻¹ at M11L/def2-TZVP and PW6B95D3/def2-TZVP levels of theory, respectively, suggesting that S(LP)···π interactions are attractive in nature. These findings are in agreement with the previous analysis of 172 crystallographic structures deposited in the Protein Data Bank, which identified 96 examples of attractive S(LP)···π(FAD) interactions, where FAD is flavin adenine dinucleotide.[39]

The results presented in Figure 10 also suggest that, except for ωb97XD/def2-TZVP predictions for **1d-Me,SH** and **3d-Me,SH** (Figure 10b), the gauche rotamer with only one of the sulfur lone pairs oriented towards the π(Arene) or π(Alkene) moieties is strongly disfavoured in the **Me,SH** balances compared to the **Me,OH** balances and the conformational equilibrium has reduced to a two-site equilibrium between the eclipsed and trans-rotamers. From further calculations for individual rotamers with full geometry optimisations and frequency calculations, the M11L/def2-TZVP predicted populations of the eclipsed rotamer are 61.4% for **1d-Me,SH** and 85.3% for **4d-Me,SH**. The eclipsed rotamer is preferred by the free energy difference of −1.15 and −4.35 kJ mol⁻¹ for **1d** and **4d**, respectively, compared to the corresponding trans rotamer. The predicted populations of the eclipsed rotamer by PW6B95D3/def2-TZVP are 37.4% for **1d-Me,SH** and 74.0% for **4d-Me,SH**, with the corresponding free energies of +1.27 and −2.58 kJ mol⁻¹ in **1d** and **4d**, respectively, for the eclipsed rotamer compared to the corresponding trans rotamer. At the PW6B95D3/def2-QZVPP level of theory, the predicted populations of the eclipsed rotamer are 32.1% for **1d-Me,SH** and 73.6% for **4d-Me,SH**, with the corresponding free energies of +1.86 and −2.54 kJ mol⁻¹ in **1d** and **4d**, respectively, for the eclipsed rotamer compared to the corresponding trans rotamer. The results for **4d-Me,SH** from ωB97XD/def2-TZVP are in qualitative agreement with the PW6B95D3/def2-TZVP predictions, that is, a two-site exchange occurs between the eclipsed (population 42.7% with the free energy of +0.73 kJ mol⁻¹ relative to the trans rotamer) and trans rotamers (population 57.3%). For **1d-Me,SH**, however, the eclipsed conformer appears as a transition state between two gauche rotamers (19.0% each with the free energy of +2.93 kJ mol⁻¹ relative to the trans rotamer), which are in turn in equilibrium with the dominant trans rotamer (62.0%). However, considering that PW6B95D3 performs significantly better than ωB97XD (Tables 1 and 2), a two-site exchange between eclipsed and trans rotamers is likely to be true for **1d-Me,SH**.

Electrostatic Potentials. In an attempt to clarify the preference of different conformers on simulations of OH and SH group rotations, we have calculated molecular electrostatic potentials (MESPs) of H₂O and H₂S molecules, which show distinct differences (Figure 11). In particular, the two lone pairs appear as a single red ellipsoid for the oxygen atom (with the highest negative value of −0.0431 au) and as two separate red ellipsoids for the sulfur atom (with the highest negative value of −0.0210 au). In the middle between the two red ellipsoids in H₂S, the ESP value is −0.0097 au, which is significantly more positive than at the same point in H₂O (-0.0431 au). Overall, at any point on the MESP surface, the ESP values are significantly
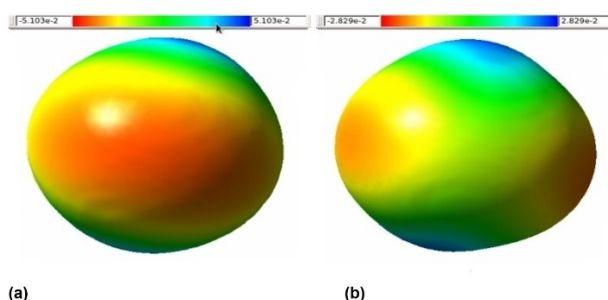

Figure 11. Calculated molecular electrostatic potentials (MESPs) of (a) H₂O and (b) H₂S at the HF/aug-cc-pVTZ level of theory.

more positive for H₂S compared to H₂O. Thus, MESP calculations suggest that the S···π interaction is expected to be more stabilising than the O···π interaction. An additional characteristic to consider is the chameleonic nature of the sulfur atom which is capable of changing its electron density distribution depending on its surrounding, which is addressed in the following section.

Electron-withdrawing vs. electron-donating groups. Further insight into S···π(Arene) interactions can be gained by introducing electron-withdrawing groups into one of the aromatic rings. For both tetrachloro and tetranitro derivatives **8** and **9**, respectively, shown in Figure 12, the conformer in which the sulfur atom points towards the electron deficient aromatic ring is preferred.

The calculated populations of the preferred conformers shown in Figure 12 are 74.7% (ωB97XD/def2-TZVP), 78.2% (M11L/def2-TZVP), 83.4% (PW2B95D3/def2-TZVP) and 82.6% (PW2B95D3/def2-QZVPP) for the tetrachloro derivative and 85.6% (ωB97XD/def2-TZVP), 88.3% (M11L/def2-TZVP), 94.9% (PW2B95D3/def2-TZVP) and 93.5% (PW2B95D3/def2-QZVPP) for the tetranitro derivative. These findings are in favour of the attractive nature of S(LP)···π(Arene) interactions, where the decrease of the electron density above the aromatic ring leads to stronger S(LP)···π(Arene) interactions. Surprisingly, however, the introduction of electron-donating hydroxyl groups also led to the preferred conformer in which the sulfur atom points towards the electron-rich aromatic ring with hydroxyl groups in the tetra-hydroxy derivative **10**: 84.8% (ωB97XD/def2-TZVP), 72.4% (M11L/def2-TZVP), 85.5% (PW2B95D3/def2-TZVP) and 82.3% (PW2B95D3/def2-QZVPP). These findings are in agreement with the experimental results[29] and confirm the ability of sulfur to act as an atomic chameleon, which is capable of
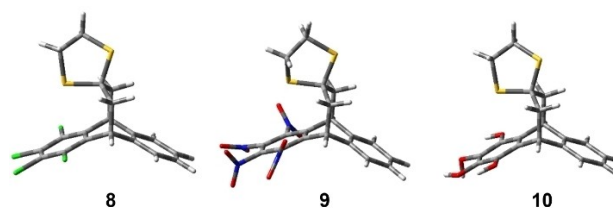

Figure 12. Tetra (**8–10**) substituted balances. The preferred conformer as predicted by DFT calculations is shown in each case.

Chemistry—Methods

Research Article
doi.org/10.1002/cmtd.202200044

**Chemistry
Europe**
European Chemical
Societies Publishing

Table 4. Percentage populations of conformers in which the sulfur atom points towards the substituted aromatic ring.

Compound	The aromatic ring substitution	M11L def2-TZVP	ωB97XD def2-TZVP	PW6B95D3 def2-TZVP
11	1-Cl	78.2	54.2	83.1
12	2-Cl	59.7	43.9	67.6
13	1,3-Cl	76.4	59.7	74.5
14	2,3-Cl	53.3	61.9	63.2
15	1,2,3-Cl	76.6	61.1	88.5
16	1,2,4-Cl	79.7	60.2	83.0
8	1,2,3,4-Cl	78.2	74.7	83.4
17	1-OH	68.2	48.3	63.3
18	2-OH	45.5[a]	45.3[a]	75.8[a]
19	1,3-OH	74.4	52.9	68.2
20	2,3-OH	61.4	54.5	72.1
21	1,2,3-OH	56.0	65.9	77.0
22	1,2,4-OH	69.6	66.8	74.1
10	1,2,3,4-OH	72.4	84.8	85.5

[a] From PW6B95D3/def2-QZVPP calculations, the population of the conformer in which the sulfur atom points towards the substituted aromatic ring is 76.4%.

rearranging its electronic surrounding in order to form an attractive interaction with various π systems, including those with either electron-donating or electron-withdrawing groups. A gradual increase of the number of substituents on the OH- and Cl-substitution of one of the aromatic rings was also considered (Table 4). With the exception of four predictions (shown in bold in Table 4) by the ωB97XD and M11L functionals for mono-substituted derivatives, in all other cases the sulfur atom was predicted to point towards the substituted aromatic ring in the preferred conformer with the populations varying between 60–88% for the Cl-substitution and 56–86% for the OH substitution (Table 4).

Conclusions

The use of 1D PES acquired by performing hydroxyl and thiol group rotation scans was shown to be a powerful tool to allow for both qualitative and quantitative analysis of noncovalent interactions. Different levels of theory examined in this work showed important differences in reliability of different DFT methods in reproducing experimental results. Overall, the results obtained in this work show that certain DFT methods can be used for quantitative or semi-quantitative assessments of the strengths of different noncovalent interactions. Synthesis of each molecular balance involves multiple steps, as described previously.[25–29] Therefore, a reliable computational approach identified in this work is useful prior to the lengthy synthesis of new balances to compare various combinations of functional groups.

Based on the analysis of the results, we have selected PW6B95D3 functional with def2-TZVP basis set, which best reproduces the experimental data for various functional groups noncovalently interacting with π systems. Two other functionals, ωB97XD and M11L, performed slightly worse than PW6B95D3 in reproducing the available experimental data. The simulation of the rotation of the hydroxyl group allowed to

reveal stabilising OH⋯Alkyne and OH⋯Nitrile noncovalent interactions that are difficult to identify experimentally. The best performing DFT methods were then applied to compare the strengths of sulfur⋯π interactions in different molecular balances which have not been explored experimentally. The simulation of the thiol group rotation showed that the conformer with the two lone pairs of the sulfur atom oriented towards the aromatic ring or the double bond is significantly stabilised, allowing to establish the directionality of sulfur⋯π interactions, which was previously not available from experimental measurements. The ability of sulfur to rearrange its electronic surrounding in order to form an attractive interaction with various π systems, including those with either electron-donating or electron-withdrawing groups, was also confirmed.

Computational Details

Different molecular structures used as balances were created and modified using the PCModel program (version 8.5).[40] These structures were then minimised using the MMX force field of the PCModel program. The structures were visualised and further modified using GaussView (version 6).[41] DFT calculations were carried out using the *Gaussian 16* program (revision A.03).[42] The following functionals were used: M11L,[43] M06-2X,[44] ωB97XD,[45] PW6B95D3[46] and MN15.[32] The basis sets used were def2-TZVP,[47] def2-TZQZPP[47] and 6–31+G(d).[48] The ultrafine numerical integration grid (with 99 radial shells and 590 angular points per shell) was used in DFT geometry optimisations, combined with the "verytight" convergence condition (requesting the root-mean-square forces to be smaller than 1×10^{-6} hartree bohr^{-1}). Frequency calculations were subsequently carried out at the same level of theory from which the Gibbs free energies were derived. These calculations were also used to verify that the optimized geometries correspond to true minima by checking whether any imaginary frequency was encountered. On calculating populations from free energies, the harmonic oscillator and rigid rotor models were used. No scaling of calculated frequencies were undertaken and as-calculated frequencies were used (for possible sources of error associated with the use of unscaled frequencies, see Alecu et al.[49] The optimised final

molecular geometries were also used to produce wavefunction files using the *Gaussian 16* program, which were used afterwards for DDEC6 calculations using the *Chargemol* program.[50] DFT calculations were carried out in which a stepwise rotation around the O—C bond was simulated. Chloroform solvent effects were included in all calculations using the integral equation formalism of the polarizable continuum model (IEFPCM), which is the default SCRF (Self-Consistent Reaction Field) method implemented in *Gaussian 16*.[51]

For conformer population calculations, the equilibrium constant was derived from the Gibbs free energy of formation [Eq. (1)]:

$$K = e^{-\frac{\Delta G^{\circ}}{RT}} \tag{1}$$

where R is the universal gas constant and T is the temperature of the system. For the two-site exchange, the equilibrium constant is defined as [Eq. (2)]:

$$K = \frac{p_1}{p_2} \tag{2}$$

where p_1 (in %) is the population of the preferred conformer. By calculating the Gibbs free energy differences (ΔG°) using DFT methods and using above two equations, conformer populations were calculated. For multi-site exchange models, the relative free energies of conformers relative to that of the trans Z-up conformer were calculated, which were then used to calculate the corresponding K values and populations. In particular, an exchange between 6 conformers was considered for **1**–**4** of H|OH, Me|OH, At|OH and CN|OH (Figure 7). A two-site exchange was considered for **5**–**22** (Figure 8) and for **1d** and **4d** of Me|SH.

Acknowledgements

Conflict of Interest

The authors declare no conflict of interest.

Data Availability Statement

The data that support the findings of this study are available in the supplementary material of this article.

[1] a) V. G. Lafitte, A. E. Aliev, P. N. Horton, M. B. Hursthouse, H. C. Hailes, *Chem. Commun.* **2006**, 2173–2175; b) A. S. Mahadevi, G. N. Sastry, *Chem. Rev.* **2016**, *116*, 2775–2825.

[2] a) A. D. Hughes, E. V. Anslyn, *Proc. Natl. Acad. Sci. USA* **2007**, *104*, 6538–6543; b) C. C. J. Loh, *Nat. Chem. Rev.* **2021**, *5*, 792–815.

[3] a) I. G. Grosu, X. Filip, M. O. Miclăuş, C. Filip, *Molecules* **2020**, *25*, 3757; b) I. Alkorta, J. Elguero, A. Frontera, *Crystals* **2020**, *10*, 180.

[4] a) K. Muller-Dethlefs, P. Hobza, *Chem. Rev.* **2000**, *100*, 143–168; b) Y. S. Al-Hamdani, A. Tkatchenko, *J. Chem. Phys.* **2019**, *150*, 010901; c) S. E. Wheeler, J. W. G. Bloom, *J. Phys. Chem. A* **2014**, *118*, 6133–6147; d) J. Hwang, P. Li, M. D. Smith, C. E. Warden, D. A. Sirianni, E. C. Vik, J. M. Maier, C. J. Yehl, C. D. Sherrill, K. D. Shimizu, *J. Am. Chem. Soc.* **2018**, *140*, 13301–13307.

[5] D. B. Amabilino, J. F. Stoddart, *Chem. Rev.* **1995**, *95*, 2725–2828.

[6] J. Clayden, *Chem. Soc. Rev.* **2009**, *38*, 817–829.

[7] J. M. Lehn, *Science* **2002**, *295*, 2400–2403.

[8] A. T. Krueger, E. T. Kool, *Curr. Opin. Chem. Biol.* **2007**, *11*, 588–594.

[9] S. Deechongkit, H. Nguyen, E. T. Powers, P. E. Dawson, M. Gruebele, J. W. Kelly, *Nature* **2004**, *430*, 101–105.

[10] J. Cerny, P. Hobza, *Phys. Chem. Chem. Phys.* **2007**, *9*, 5291–5303.

[11] a) S. Tsuzuki, *Interactions with Aromatic Rings in Structure, Bonding*, Springer, Berlin/Heidelberg, **2005**, vol. 115, pp. 149–193; b) S. E. Wheeler, *Acc. Chem. Res.* **2013**, *46*, 1029–1038.

[12] I. K. Mati, S. L. Cockroft, *Chem. Soc. Rev.* **2010**, *39*, 4195–4205.

[13] A. E. Aliev, W. B. Motherwell, *Chem. Eur. J.* **2019**, *25*, 10516–10530.

[14] M. Ōki, *Acc. Chem. Res.* **1990**, *23*, 351–356.

[15] S. Paliwal, S. Geib, C. S. Wilcox, *J. Am. Chem. Soc.* **1994**, *116*, 4497–4498.

[16] E. Kim, S. Paliwal, C. S. Wilcox, *J. Am. Chem. Soc.* **1998**, *120*, 11192–11193.

[17] B. Bhayana, C. S. Wilcox, *Angew. Chem. Int. Ed. Engl.* **2007**, *46*, 6833–6836.

[18] F. Cozzi, J. S. Siegel, *Pure Appl. Chem.* **1995**, *67*, 683–689.

[19] F. Cozzi, R. Annunziata, M. Benaglia, M. Cinquini, L. Raimondi, K. K. Baldridge, J. S. Siegel, *Org. Biomol. Chem.* **2003**, *1*, 157–162.

[20] F. Cozzi, R. Annunziata, M. Benaglia, K. K. Baldridge, G. Aguirre, J. Estrada, Y. Sritana–Anant, J. S. Siegel, *Phys. Chem. Chem. Phys.* **2008**, *10*, 2686–2694.

[21] S. M. Verma, N. B. Singh, *Aust. J. Chem.* **1976**, *29*, 295–300.

[22] W. B. Jennings, B. M. Farrell, J. F. Malone, *J. Org. Chem.* **2006**, *71*, 2277–2282.

[23] W. B. Jennings, N. O'Connell, J. F. Malone, D. R. Boyd, *Org. Biomol. Chem.* **2013**, *11*, 5278–5291.

[24] K. B. Muchowska, C. Adam, I. K. Mati, S. L. Cockroft, *J. Am. Chem. Soc.* **2013**, *135*, 9976–9979.

[25] W. B. Motherwell, J. Moise, A. E. Aliev, M. Nič, S. J. Coles, P. N. Horton, M. B. Hursthouse, G. Chessari, C. A. Hunter, J. G. Vinter, *Angew. Chem. Int. Ed. Engl.* **2007**, *46*, 7823–7826.

[26] A. E. Aliev, J. Moise, W. B. Motherwell, M. Nič, D. Courtier-Murias, D. A. Tocher, *Phys. Chem. Chem. Phys.* **2009**, *11*, 97–100.

[27] A. E. Aliev, J. R. Arendorf, I. Pavlakos, R. B. Moreno, M. J. Porter, H. S. Rzepa, W. B. Motherwell, *Angew. Chem. Int. Ed. Engl.* **2015**, *54*, 551–555.

[28] I. Pavlakos, T. Arif, A. E. Aliev, W. B. Motherwell, G. J. Tizzard, S. J. Coles, *Angew. Chem. Int. Ed. Engl.* **2015**, *54*, 8169–8174.

[29] W. B. Motherwell, R. B. Moreno, I. Pavlakos, J. R. T. Arendorf, T. Arif, G. J. Tizzard, S. J. Coles, A. E. Aliev, *Angew. Chem. Int. Ed.* **2018**, *57*, 1193–1198; *Angew. Chem.* **2018**, *130*, 1207–1212.

[30] a) T. A. Manz, *RSC Adv.* **2017**, 7, 45552–45581; b) T. A. Manz, N. G. Limas, *RSC Adv.* **2016**, 6, 47771–47801; c) N. G. Limas, T. A. Manz, *RSC Adv.* **2016**, *6*, 45727–45747; d) N. G. Limas, T. A. Manz, *RSC Adv.* **2018**, 8, 2678–2707.

[31] A. E. Aliev, S. Bhandal, D. Courtier-Murias, *J. Phys. Chem. A* **2009**, *113*, 10858–10865.

[32] H. S. Yu, X. He, S. L. Li, D. G. Truhlar, *Chem. Sci.* **2016**, *7*, 5032–5051.

[33] Other charge models may give more accurate results than the DDEC analysis, see B. Wang, S. L. Li, D. G. Truhlar, *J. Chem. Theory Comput.* **2014**, *10*, 5640–5650.

[34] C. R. Forbes, S. K. Sinha, H. K. Ganguly, S. Bai, G. P. A. Yap, S. Patel, N. J. Zondlo, *J. Am. Chem. Soc.* **2017**, *139*, 1842–1855.

[35] D. Pal, P. Chakrabarti, *J. Biomol. Struct. Dyn.* **2001**, *19*, 115–128.

[36] U. Samanta, D. Pal, P. Chakrabarti, *Proteins* **2000**, *38*, 288–300.

[37] A. R. Viguera, L. Serrano, *Biochemistry* **1995**, *34*, 8771–8779.

[38] K. N.-M. Daeffler, H. A. Lester, D. A. Dougherty, *J. Am. Chem. Soc.* **2012**, *134*, 14890–14896.

[39] R. F. N. Silva, A. C. S. Sacco, I. Caracelli, J. Zukerman-Scpector, E. R. T. Tiekink, *Z. Kristallogr.* **2018**, *233*, 531–537.

[40] K. E. Gilbert, J. J. Gajewski, PCMODEL version 8.5, Molecular Modeling Software for Windows Operating System, Apple Macintosh OS, Linux, Unix. Serena Software.

[41] GaussView, Version 6, R. Dennington, T. Keith, J. Millam, Semichem Inc., Shawnee Mission, KS, 2016.

[42] Gaussian 16, Revision A.03, M. J. Frisch, G. W. Trucks, H. B. Schlegel, G. E. Scuseria, M. A. Robb, J. R. Cheeseman, G. Scalmani, V. Barone, G. A. Petersson, H. Nakatsuji, X. Li, M. Caricato, A. V. Marenich, J. Bloino, B. G. Janesko, R. Gomperts, B. Mennucci, H. P. Hratchian, J. V. Ortiz, A. F. Izmaylov, J. L. Sonnenberg, D. Williams-Young, F. Ding, F. Lipparini, F. Egidi, J. Goings, B. Peng, A. Petrone, T. Henderson, D. Ranasinghe, V. G. Zakrzewski, J. Gao, N. Rega, G. Zheng, W. Liang, M. Hada, M. Ehara, K. Toyota, R. Fukuda, J. Hasegawa, M. Ishida, T. Nakajima, Y. Honda, O. Kitao, H. Nakai, T. Vreven, K. Throssell, J. A. Montgomery, Jr., J. E. Peralta, F. Ogliaro, M. J. Bearpark, J. J. Heyd, E. N. Brothers, K. N. Kudin, V. N. Staroverov, T. A. Keith, R. Kobayashi, J. Normand, K. Raghavachari, A. P. Rendell, J. C. Burant, S. S. Iyengar, J. Tomasi, M. Cossi, J. M. Millam, M. Klene, C. Adamo, R. Cammi, J. W. Ochterski, R. L. Martin, K. Morokuma, O. Farkas, J. B. Foresman, D. J. Fox, Gaussian, Inc., Wallingford CT, 2016.

[43] R. Peverati, D. G. Truhlar, *J. Phys. Chem. Lett.* **2012**, *3*, 117–124.

[44] Y. Zhao, D. G. Truhlar, *Theor. Chem. Acc.* **2008**, *120*, 215–241.

[45] J.-D. Chai, M. Head-Gordon, *Phys. Chem. Chem. Phys.* **2008**, *10*, 6615–6620.

[46] Y. Zhao, D. G. Truhlar, *J. Phys. Chem. A* **2005**, *109*, 5656–5667.

[47] a) F. Weigend, R. Ahlrichs, *Phys. Chem. Chem. Phys.* **2005**, *7*, 3297–3305; b) F. Weigend, *Phys. Chem. Chem. Phys.* **2006**, *8*, 1057–1065.

[48] V. A. Rassolov, M. A. Ratner, J. A. Pople, P. C. Redfern, L. A. Curtiss, *J. Comb. Chem.* **2001**, *22*, 976–984.

[49] I. M. Alecu, J. Zheng, Y. Zhao, D. G. Truhlar, *J. Chem. Theory Comput.* **2010**, *6*, 2872–2887.

[50] T. A. Manz, N. G. Limas, *Chargemol program for performing DDEC analysis*, http://ddec.sourceforge.net/.

[51] a) E. Cances, B. Mennucci, *J. Math. Chem.* **1998**, *23*, 309–326; b) M. Cossi, N. Rega, G. Scalmani, V. Barone, *J. Comb. Chem.* **2003**, *24*, 669–681.

RESEARCH ARTICLE

Molecular balances are used to compare noncovalent interactions. However, some balances are difficult to make. In this work, noncovalent interactions of π systems are probed using various DFT methods and it is shown that the PW6B95D3 functional reproduces best the experimental data. Then the strengths of sulfur···π interactions are compared in molecules which have not been explored experimentally.

L. Nunar, Dr. A. E. Aliev*

1 – 14

Quantification of the Strength of π-Noncovalent Interactions in Molecular Balances using Density Functional Methods